Deuterium metabolic imaging of Alzheimer's disease at 3-T magnetic-field strength: A pilot case–control study

Alixander S. Khan, [1] Katie A. Peterson, [1] Orsolya Vittay, [2] Mary McLean, [1] Joshua Kaggie, [1] John T. O'Brien, [3] James B. Rowe, [4] Ferdia A. Gallagher, [1,2] and Tomasz Matys[1,2]

Author Affiliations:

1 Department of Radiology, University of Cambridge, Cambridge, CB2 0QQ, United Kingdom

2 Department of Radiology, Cambridge University Hospitals NHS Foundation Trust, Cambridge, CB2 0QQ, United Kingdom

3 Department of Psychiatry, University of Cambridge, Cambridge, CB2 0SZ, United Kingdom

4 Department of Clinical Neurosciences, University of Cambridge, Cambridge, CB2 0QQ, United Kingdom

The work originated from the Department of Radiology, Hills Road, University of Cambridge, Cambridge, CB2 0QQ

Corresponding author: Dr Tomasz Matys

Department of Radiology, Hills Road, University of Cambridge, Cambridge, CB2 0QQ

Telephone number: 0044 1223 336894, e-mail: tm418@cam.ac.uk

Funding Information

The study was funded by the Evelyn Trust grant number 20/26. This research was supported by the NIHR Cambridge Biomedical Research Centre (NIHR203312). The authors are supported by funding from Cancer Research UK. AK is supported by Lubeck Foundation. JBR is supported by the Wellcome Trust (220258), the Medical Research Council and Dementias Platform UK (MC_UU_00030/14; MR/T033371/1). The views expressed are those of the authors and not necessarily those of the NIHR or the Department of Health and Social Care.

Manuscript Type - Original Research

Word Count for Text – 3288

List of abbreviations:

AD - Alzheimer's disease, DMI - deuterium metabolic imaging, MRS - magnetic resonance spectroscopy, MRSI - magnetic resonance spectroscopy imaging

Summary statement:

Deuterium metabolic imaging (3 T) demonstrated reductions in oxidative glucose metabolism at whole-brain spectroscopy, but no evidence of regional signal changes, in participants with Alzheimer's disease .

Key results:

In this prospective case–control pilot study of ten patients with symptomatic Alzheimer's disease (AD) and nine cognitively healthy control individuals, 3-T deuterium metabolic imaging (DMI) demonstrated a lower peak ^{2}H-glutamate/glutamine-to-^{2}H-glucose signal ratio in participants with AD than in controls (*P*=.04) on whole-brain spectroscopy, suggesting oxidative glucose metabolism impairment in AD.

There was no evidence of regional signal differences in participants with AD at 3-T DMI magnetic resonance spectroscopy imaging.

Abstract

Background: Impaired glucose metabolism is characteristic of several dementia types, preceding cognitive symptoms and structural brain changes. Reduced glucose uptake detection in specific brain regions using ^{18}F-fluorodeoxyglucose-PET (^{18}F-FDG-PET) is a valuable diagnostic marker in Alzheimer's disease (AD). However, ^{18}F-FDG-PET use in clinical practice may be limited by equipment availability and high cost.

Purpose*:* To test the feasibility of using MRI-based deuterium metabolic imaging (DMI) at a clinical magnetic-field strength (3 T) to detect and localize changes in glucose and its metabolites in patients with a clinical diagnosis of AD.

Materials and Methods: Participants were recruited for this prospective case–control pilot study between March 2021 and February 2023. DMI was performed at 3 T using a custom birdcage head coil following oral administration of deuterium-labeled glucose (0.75 g/kg). Unlocalized whole-brain magnetic resonance spectroscopy (MRS) and 3D magnetic resonance spectroscopic images (MRSI, cubic 3.2 cm voxel) were acquired. Ratios of ^{2}H-glucose, ^{2}H-glutamate/glutamine (^{2}H-Glx) and ^{2}H-lactate spectroscopic peak signals to ^{2}H-water peak signal were calculated for the whole-brain MRS, and for individual MRSI voxels.

Results: A total of 19 participants, including 10 participants with AD (mean age, 68 years ±5 [SD]; 8 males) and 9 cognitively healthy control participants (mean age, 70 years ± 6 [SD]; 6 males) were evaluated. Whole-brain spectra demonstrated a reduced ratio of the peak ^{2}H-Glx to ^{2}H-glucose signals in participants with AD compared with control participants (0.41±0.09 vs. 0.58±0.20, *P*=.04), suggesting an impairment of oxidative glucose metabolism in AD. However, there was no evidence of localization of these changes to the expected regions of metabolic impairment on MRSI presumably due to insufficient spatial resolution.

Conclusion: DMI at 3 T demonstrated impairment of oxidative glucose metabolism in patients with Alzheimer's disease but no evidence of regional signal differences.

Introduction

Dementia is an important public health problem with an increasing burden on healthcare and social care systems (1). The most common cause of dementia, accounting for approximately 65% of cases, is Alzheimer's disease (AD)(2). Early diagnosis of AD is central for initiating treatment and mitigating cognitive decline and is becoming particularly important with new targeted pharmacological treatments (3). The diagnosis of dementia increasingly relies on diagnostic markers (3,4). One early finding in AD is glucose uptake reduction in the posterior cingulate and temporoparietal regions which can be detected by PET with the glucose analog ^{18}F-fluorodeoxyglucose (^{18}F-FDG-PET)(5,6). ^{18}F-FDG-PET has been demonstrated as a useful method for diagnosing AD and predicting the disease course (5–7) and is especially recommended when the etiology of dementia is unclear (4,8). However, its use remains limited by the higher cost and lower availability of PET than MRI (5).

Deuterium metabolic imaging (DMI) is an emerging method of imaging tissue metabolism based on magnetic resonance spectroscopic (MRS) detection of deuterium-labeled compounds, most often glucose. Using deuterium for spectroscopic imaging has several technical advantages. Owing to the low abundance of natural deuterium (0.0156%), the need for background water and lipid suppression is avoided, and a low gyromagnetic ratio of deuterium reduces the sensitivity to magnetic field inhomogeneities (9,10). The negative impact of a lower resonance frequency on the signal-to-noise ratio (SNR) is partly offset by a spin quantum number of 1 and short relaxation times, which allows repeated acquisition within a reasonable scan time (9,10). Following preclinical experiments (9), translation of DMI into humans has demonstrated successful detection and mapping of ^{2}H-glucose in the healthy brain and in patients with glioma after oral administration (10). In addition, the detection of downstream metabolites, combined ^{2}H-glutamate/glutamine (^{2}H-Glx) and ^{2}H-lactate, provides indirect

measures of the activities of the oxidative phosphorylation and reductive glycolytic pathways, respectively (10). Thus, DMI offers data on glucose metabolic flux that are not available using ^{18}F-FDG-PET, in which the glucose analog is not fully metabolized and accumulates within the cell (6). The simplicity of using orally administered and nonradioactive ^{2}H-glucose offers important advantages for potential practical usability.

In the initial DMI studies in humans, experimental magnetic fields of 4 T (10) and 9.4 T (11) were used. However, it has been recently demonstrated that DMI can be performed on a 3-T MRI system (12,13), which could facilitate its use in clinical settings, as the widely available 3-T scanners would require only a coil tuned to the deuterium resonance frequency and multinuclear capabilities with relevant pulse sequences (12). Given the evidence of glucose metabolism dysregulation in AD, we hypothesized that 3-T DMI could be useful as a diagnostic marker. The aim of this study was to test the feasibility of 3-T DMI to detect and localize changes in glucose and its metabolites in patients with a clinical diagnosis of AD.

Materials and methods

Participant characteristics

The prospective case–control pilot study, performed between March 2021 and February 2023, was approved by the NHS Research Ethics Committee (20/NE/0232), and all participants provided informed consent. Brain DMI was performed in 10 randomly selected patients with symptomatic AD and 10 control participants over 60 years of age. Patients were recruited from the Cambridge University Hospitals NHS Trust Memory Clinic and the National Institutes of Health (NIHR) Join Dementia Research Register. All patients had an established diagnosis of probable AD based on National Institute on Aging (NIA) criteria (8,14) following comprehensive examination by a specialist neurologist (JBR, 19 years experience) or a psychiatrist (JTO, 30 years experience), including clinical assessment, cognitive evaluation using the Addenbrooke Cognitive Examination Revised (ACE-R) test (15), and

structural brain imaging. ^{18}F-FDG-PET and cerebrospinal fluid markers are not routinely used in the UK (8) but are reported where available. Healthy volunteers were recruited from the NIHR Join Dementia Research Register, memory clinics (nonrelated carers of dementia patients) and poster advertisements on the study institution campus based on the absence of cognitive symptoms, and were further evaluated using a Test Your Memory (TYM) screening test (16), included in the UK national guidelines (8) and routinely used in memory services for its high negative predictive value for AD (16) and non-AD dementia (17). The exclusion criteria included diabetes, a psychiatric or neurological diagnosis other than AD, and insufficient MRS quality.

DMI acquisition

DMI was performed using a 3-T MRI system (MR750; GE Healthcare) used in research mode with multinuclear capabilities. Deuterated glucose ([6,6′-$^{2}H_2$]glucose, Cambridge Isotopes Laboratories) was dissolved in 200 ml of water and given orally (0.75 g/kg, maximum 60 g) after at least 6 hours of fasting. The study timeline is shown in Fig. 2. Following structural proton brain MRI (sagittal 3D Cube T1, 0.7x0.7x1.0 mm and 3D FLAIR, 0.7x0.7x0.7 mm) using a standard head coil (operating at ^{1}H resonant frequency, 127.78 MHz at 3 T), the patient was removed from the scanner. The coil was changed to a single-tuned four-rung birdcage DMI coil with a 30 cm diameter and 24 cm rung length (GE 1.5 T phosphorus head coil modified to operate at a ^{2}H resonant frequency, 19.61 MHz at 3 T). Shimming was performed over an ellipsoid region including most of the brain using the body coil with the DMI coil in position. T1-weighted spoiled gradient echo images (1.0x1.0x2.0 mm) were obtained using the body coil . Eddy current settings were adjusted for ^{2}H, and Bloch-Siegert radiofrequency calibration measurements were performed to determine the transmit power and imaging frequencies (12). 3D magnetic resonance spectroscopic imaging (MRSI) spectra were obtained 87±14 min after glucose consumption (84±11 min for control participants and 89±14 min for participants with AD) using a pulse-acquire sequence with 32 cm field of view, 10×10×10 matrix (voxel size 3.2 cm cubic), TR of 120 ms, 5000 Hz, and 544 points. A nominal 90° flip angle was used, providing an effective flip angle of 45°

close to the Ernst angle of ^{2}H-water of 46.6° assuming a T1 of 320 ms. The scan parameters were based on a previous study to provide an optimal SNR within 10 min scan duration, allowing the presence of saturation effects correctable during postprocessing (12). Unlocalized (whole-brain) MRS spectra were obtained at a mean time of 94±14 min after glucose consumption (92±12 min for control participants and 97±15 min for participants with AD) using a 90° nominal flip angle, 1-s TR, 128 averages, 5000 Hz, 2048 points, and 128-s scan duration; at this TR, saturation effects are negligible. In most participants (n=17), a repeat unlocalized measurement was obtained 13±3 min before (n=15) or after (n=2) this timepoint.

Data evaluation

Spectroscopic data were analyzed in MATLAB using OXSA AMARES 2.0 (18) by ASK (3 years experience). The ^{2}H-water (4.7 ppm), ^{2}H-glucose (3.9 ppm), ^{2}H-Glx (2.4 ppm) and ^{2}H-lactate (1.35 ppm) peak signals were obtained. Metabolite ratios were normalized to water to account for nonuniformities in coil sensitivity by dividing the signals by ^{2}H-water signal (12). Percentage change in ^{2}H-water signal over time was calculated by dividing the change in signal amplitude by the initial signal and the time between two MRS acquisitions. Structural imaging was visually rated by a neuroradiologist blinded to the experimental group (TM, 9 years experience). Medial temporal atrophy (MTA) was graded on coronal T1 reconstructions using the Scheltens scale (19); MTA ≥2 at <75 years or ≥3 at any age was considered characteristic of AD (19). The degree of small vessel disease was graded on axial FLAIR reconstructions using the Fazekas scale (20). MRSI data analysis is described in Appendix 1.

Statistical analysis

Data are expressed as the mean ± standard deviation. Data were tested for normality using the Kolmogorov-Smirnov test. The Student t-test was used for between-groups comparisons for normally distributed data, otherwise the Mann-Whitney test was applied. Correlations involving continuous and discrete variables were tested using Pearson or Spearman correlations, respectively. Statistical

significance was assumed at a *P* value of less than 0.05 (two-tailed). Statistical analysis was performed using IBM SPSS v29.

Results

Participant characteristics

Ten AD patients and ten control participants were recruited and scanned but one control participant was excluded from the analysis due to insufficient MRS quality (Fig. 1). The demographic and clinical data of the included participants (ten AD patients, mean age, 68 years ±5 [SD]; 8 males, 2 females, and nine control participants, 70 years ±6 [SD]; 6 males, 3 females) are shown in Table 1 and Supplemental Table 1. Structural changes characteristic of AD were present in eight participants with AD; two participants with AD had minimal medial temporal atrophy, but one had positive cerebrospinal fluid markers for AD, and one had a positive ^{18}F-FDG-PET scan (Supplemental Table 1). None of the control participants showed medial temporal lobe atrophy or cognitive impairment. Fazekas grades were comparable between participants with AD (1.3±0.5) and controls (1.4±0.5, *P*=.54); none of the participants had previous large vessel territories or strategic lacunar infarcts.

DMI results

Whole-brain MRS detected ^{2}H-water, ^{2}H-glucose, ^{2}H-Glx and ^{2}H-lactate peaks in all participants. Examples of whole-brain spectra obtained from a participant with AD and control participant are shown in Fig. 3.

There was no evidence of a difference between participants with AD and controls for whole-brain ^{2}H-glucose/^{2}H-water (0.50±0.07 vs. 0.43±0.10; *P*=.09), ^{2}H-Glx/^{2}H-water (0.20±0.05 vs. 0.24±0.07; *P*=.24) or ^{2}H-lactate/^{2}H-water ratios (0.05±0.03 vs. 0.06±0.05; *P*=.56). The whole-brain ratio of ^{2}H-Glx/^{2}H-glucose was lower in patients with AD than in controls (0.41±0.09 vs. 0.58 ± 0.20, *P*=.04), suggesting an impairment of oxidative glucose metabolism. The ratio of ^{2}H-lactate/^{2}H-glucose was similar between

the groups (0.11±0.07 vs 0.14±0.10, *P*=.44; Fig. 4). No correlations were found between these parameters and the degree of cognitive impairment (ACE-R) or structural atrophy measures (MTA grade) (Supplemental Table 2).

As an additional indirect marker of complete ^{2}H-glucose oxidation, the rate of increase in the ^{2}H-water signal was compared between two repeat whole-brain MRS acquisitions. The rate of ^{2}H-water signal increase was lower in participants with AD (0.19±0.06%/min) than in control participants (0.69±0.32%/min), although the difference did not reach statistical significance (*P*=.17).

MRSI maps of ^{2}H-glucose and its metabolites revealed relatively uniform profiles across the brain in participants with AD (Fig. 5) and control participants. There was no evidence of differences in glucose or metabolite ratios in participants with AD in comparisons of voxels overlying the areas of expected areas of glucose hypometabolism or in atlas-based regions (Appendix 1).

Discussion

Glucose hypometabolism is a recognized feature of several types of dementia (5–7). The only routine clinical imaging method directly measuring metabolic glucose information is ^{18}F-FDG-PET, which can demonstrate cellular glucose uptake but not its downstream metabolism (6). In our study, we tested the feasibility of evaluating glucose turnover in AD using 3 T DMI, which offers additional insights into glucose metabolic flux and has practical advantages that could allow its rapid clinical translation.

As in previous work in healthy volunteers (12), it was possible to resolve ^{2}H-glucose, ^{2}H-Glx and ^{2}H-lactate peaks via whole-brain spectroscopy following oral administration of ^{2}H-glucose. Participants with AD showed reduced whole-brain ^{2}H-Glx/^{2}H-glucose ratio, demonstrating an impairment of oxidative metabolism. As the complete oxidative metabolism of ^{2}H-glucose results in the incorporation of deuterium into ^{2}H-water (9), reflected in slow increase in ^{2}H-water signal over time (12), we evaluated

the rate of ^{2}H-water signal change between two MRS acquisitions as an additional marker of oxidative phosphorylation. Participants with AD demonstrated a tendency toward a lower rate of ^{2}H-water signal increase than healthy controls, in line with the ^{2}H-Glx/^{2}H-glucose results, although the difference did not reach statistical significance. This may be due to the slow ^{2}H-water signal increase after oral ^{2}H-glucose, making the measurement of the small difference between time points prone to error, and acquisitions over a longer time course may be required. As ^{2}H-water is freely diffusible, the influx of ^{2}H-water produced in other organs may also form part of the net brain signal, particularly after oral ^{2}H-glucose administration, where absorption is gradual and subject to first-pass effects. Further investigation is therefore needed to determine the usefulness of ^{2}H-water signal change as a measure of oxidative brain metabolism.

The slight increase in the global ^{2}H-glucose/^{2}H-water ratio in AD contrasts with the reduced glucose uptake on ^{18}F-FDG-PET (5–7). Although the timepoints for image acquisition after probe administration using the two techniques are similar, the different routes of administration (oral vs. intravenous) and large differences in the concentrations of the probes result in different pharmacokinetic profiles. ^{18}F-FDG-PET signal at the time of image acquisition is predominantly intracellular and localized to the cerebral cortex (6), whereas the higher net ^{2}H-glucose concentration in our whole-brain data could be due to increased extracellular, vascular or white matter content due to slower uptake. This possibility is supported by measurements in postmortem brains, which demonstrated increased glucose concentrations in cortical samples from regions susceptible to amyloid deposition in AD owing to reduced neuronal glucose transport (21). This could lead to increased extracellular ^{2}H-glucose concentration due to the larger amount of administered ^{2}H-glucose compared to tracer quantities of ^{18}F-FDG. Furthermore, analysis of ^{18}F-FDG-PET signal in white matter demonstrated a significantly higher specific binding ratio of glucose in patients with AD which correlated with amyloid accumulation, a phenomenon that may be attributed to an increased neuroinflammatory response (22). However, the

available data on the glucose metabolism in the white matter in dementia are otherwise scarce, and further investigation is warranted.

Given the relatively large regions of disturbed glucose metabolism in AD, we hoped that meaningful regional differences similar to ^{18}F-FDG-PET studies would be demonstrable on DMI despite limited resolution at 3 T (voxel volume of 33 ml achievable during 10 min scan). The detection of such topographic changes would be of particular diagnostic value, as this allows qualitative scan evaluation and differentiation of dementia types. Although in all but one participant with AD, we did not have a direct confirmation of regional glucose hypometabolism on ^{18}F-FDG-PET, its presence could be presumed because most participants with AD had established medial temporal atrophy, and metabolic changes precede structural alterations and cognitive symptoms, often by several years (6,23). However, no regional differences were detected on DMI MRSI. We assume that this was secondary to the technical limitations of the method, such as partial volume effects due to insufficient spatial resolution. However, given the different kinetics of the normally metabolized glucose in DMI, it is possible that its distribution may be different from that of nonmetabolized ^{18}F-FDG, and changes may occur in different regions or globally. The promising results from whole-brain MRS show the need for further work into DMI signal localization by improving the SNR and spatial resolution, ideally in correlation to ^{18}F-FDG-PET. Improvements in spatial resolution are achievable at 3 T through coil sensitivity optimization (13 ml with a maximum sensitivity coil) and longer acquisition times (19 ml at 30 minutes)(24); we opted for 10 min acquisition but the scan was well tolerated by all participants, and a longer scan duration is feasible. It may also be possible to combine structural MRI and DMI with little added examination time using interleaved acquisition (25). The optimal coil type for DMI is a matter of debate. Whereas 3-T studies have been performed with a birdcage coil (12,13), studies at higher magnetic field strengths have used multiarray designs (10,11,24). Birdcage coils offer simpler construction and good field homogeneity without postprocessing, and there is scope to increase the SNR by reducing resistive losses (13); however, others have suggested multiarray coils for maximum

performance (24). Our MRSI acquisition parameters, such as spherical k-space encoding and imaging close to the Ernst angle, were already similar to the proposed conditions (13). Another possibility for improving the SNR is machine learning-based denoising in postprocessing (13). Finally, discounting the practical benefits of 3 T, DMI at higher field strengths is even more promising, with 3.0-ml or 1.7-ml voxel volume achievable in 10 or 30 min, respectively, at 9.4 T and 2.7-ml in 28 min achievable at 7 T (24).

Previous studies have suggested that AD may be associated with impairment of aerobic glycolysis, in which glucose is metabolized to lactate in the presence of adequate oxygen supply (26,27). This process occurs preferentially in astrocytes, and there is evidence that lactate constitutes an important energy source for neurons through the astrocyte–lactate shuttle mechanism (28,29). Aerobic glycolysis is diminished in AD in correlation with amyloid deposition (26), preceding cognitive symptoms (27). In our study, we did not observe differences in lactate levels between participants with AD and control participants. However, the sensitivity of DMI to lactate is limited by a low signal amplitude and may be affected by lipid resonance (10,12). Other methods, such as hyperpolarized ^{13}C-MRI using pyruvate injection, may be more suitable for investigating this aspect of cerebral neuroenergetics (12).

Our pilot study has limitations. First, the trends toward increased glucose levels and smaller increases in ^{2}H-water in participants with AD were not statistically significant, likely due to the combination of relatively few participants and the low sensitivity of the technique; these findings need re-evaluation in larger studies following coil and protocol optimization. Second, while participants were not known diabetic and were asked to fast before glucose administration to ensure optimal uptake, glucose levels were not measured before the scan. It is unlikely that potential differences in glycemia influenced our results in a systematic manner. However, it would be beneficial to measure glucose levels for correlation with DMI data, and to ensure that the effects are not confounded by a metabolic disorder, especially that patients with AD may present with subclinical diabetes. Third, using water as an internal

reference could theoretically affect measured glucose and metabolite-to-water ratios because of increased cerebrospinal fluid volume secondary to a greater degree of brain atrophy in participants with AD. However, due to the high water content in the brain, atrophy has only a very small impact on the total intracranial water volume. Of key importance, the reduced Glx/glucose ratio in participants with AD is unaffected by normalization to water, as it is directly calculated from the respective peak signal heights. Fourth, as the areas of glucose hypometabolism in AD demonstrate hypoperfusion, visualization of reduced cerebral blood flow by arterial spin labeling (ASL) offers similar diagnostic performance to ^{18}F-FDG-PET and can be easily performed on the current MRI scanners (30,31). It remains to be established whether direct metabolic information from DMI could offer additional advantages. As we did not evaluate perfusion, it is also not possible to know whether the DMI findings are linked to perfusion changes, especially in the absence of regional information.

Our study adds to the body of evidence on the usability of DMI in humans (10–13, 24). For clinical translation, an important consideration would be tracer cost, which is currently considerably higher for [6,6'-$^{2}H_{2}$-]glucose than for ^{18}F-FDG. However, this price will likely decrease with increased use of the technique and larger scale production. This potential cost reduction is exemplified by recent work in which the replacement of expensive deuterides with heavy water and less demanding reaction conditions allowed a tenfold reduction in the synthesis cost (32). Moreover, a higher substitution rate (five protons replaced with deuterons) provides a higher SNR and allows potential dose reduction (32) compared with the doubly deuterated compound used in our work.

In summary, in our initial study exploring the role of DMI in AD, we demonstrated the impairment of oxidative glucose metabolism in participants with AD at 3 T, as shown by a reduced ^{2}H-Glx/^{2}H-glucose ratio on global brain spectroscopy. Further studies are needed to establish whether these changes could also be detected in the presymptomatic or prodromal stages of the disease and whether such data could support diagnostic decisions. Further investigations are warranted to determine whether DMI

could provide regional information following technical coil and scan protocol refinements sufficient to provide the necessary regional signal-to-noise ratio at 3 T or whether greater magnetic field strength would be required.

Acknowledgments

We are grateful to Mr Ashley Grimmer and Mr Matthew Locke for managerial support of the project. We thank the NIHR Join Dementia Research service (https://www.joindementiaresearch.nihr.ac.uk) for support provided during recruitment.

References

1. Alzheimer's Disease International. Dementia statistics. . https://www.alzint.org/about/dementia-facts-figures/dementia-statistics/. Accessed August 25, 2023.

2. Arvanitakis Z, Shah RC, Bennett DA. Diagnosis and Management of Dementia: Review. JAMA. 2019;322(16):1589. doi: 10.1001/jama.2019.4782.

3. Scheltens P, Strooper BD, Kivipelto M, et al. Alzheimer's disease. Lancet Lond Engl. 2021;397(10284):1577–1590. doi: 10.1016/S0140-6736(20)32205-4.

4. Chételat G, Arbizu J, Barthel H, et al. Finding our way through the labyrinth of dementia biomarkers. Eur J Nucl Med Mol Imaging. 2021;48(8):2320–2324. doi: 10.1007/s00259-021-05301-7.

5. Chételat G, Arbizu J, Barthel H, et al. Amyloid-PET and 18F-FDG-PET in the diagnostic investigation of Alzheimer's disease and other dementias. Lancet Neurol. 2020;19(11):951–962. doi: 10.1016/S1474-4422(20)30314-8.

6. Mosconi L. Glucose metabolism in normal aging and Alzheimer's disease: methodological and physiological considerations for PET studies. Clin Transl Imaging. 2013;1(4):217–233. doi: 10.1007/s40336-013-0026-y.

7. Brown RK, Bohnen NI, Wong KK, Minoshima S, Frey KA. Brain PET in suspected dementia: patterns of altered FDG metabolism. Radiographics. 2014;34(3):684–701. doi: 10.1148/rg.343135065.

8. Overview | Dementia: assessment, management and support for people living with dementia and their carers | Guidance | NICE. NICE; 2018. https://www.nice.org.uk/guidance/ng97. Accessed May 15, 2023.

9. Lu M, Zhu XH, Zhang Y, Mateescu G, Chen W. Quantitative assessment of brain glucose metabolic rates using in vivo deuterium magnetic resonance spectroscopy. J Cereb Blood Flow Metab. 2017;37(11):3518–3530. doi: 10.1177/0271678X17706444.

10. De Feyter HM, Behar KL, Corbin ZA, et al. Deuterium metabolic imaging (DMI) for MRI-based 3D mapping of metabolism in vivo. Sci Adv. 2018;4(8):eaat7314. doi: 10.1126/sciadv.aat7314.

11. Ruhm L, Avdievich N, Ziegs T, et al. Deuterium metabolic imaging in the human brain at 9.4 Tesla with high spatial and temporal resolution. Neuroimage. 2021;244:118639. doi: 10.1016/j.neuroimage.2021.118639.

12. Kaggie JD, Khan AS, Matys T, et al. Deuterium metabolic imaging and hyperpolarized ^{13}C-MRI of the normal human brain at clinical field strength reveals differential cerebral metabolism. Neuroimage. 2022;257:119284. doi: 10.1016/j.neuroimage.2022.119284.

13. Adamson PM, Datta K, Watkins R, Recht LD, Hurd RE, Spielman DM. Deuterium metabolic imaging for 3D mapping of glucose metabolism in humans with central nervous system lesions at 3T. Magn Reson Med. 2024;91(1):39–50. doi: 10.1002/mrm.29830.

14. McKhann GM, Knopman DS, Chertkow H, et al. The diagnosis of dementia due to Alzheimer's disease: recommendations from the National Institute on Aging-Alzheimer's Association workgroups on diagnostic guidelines for Alzheimer's disease. Alzheimers Dement J Alzheimers Assoc. 2011;7(3):263–269. doi: 10.1016/j.jalz.2011.03.005.

15. Mioshi E, Dawson K, Mitchell J, Arnold R, Hodges JR. The Addenbrooke's Cognitive Examination Revised (ACE-R): a brief cognitive test battery for dementia screening. Int J Geriatr Psychiatry. 2006;21(11):1078–1085. doi: 10.1002/gps.1610.

16. Brown J, Pengas G, Dawson K, Brown LA, Clatworthy P. Self administered cognitive screening test (TYM) for detection of Alzheimer's disease: cross sectional study. BMJ. British Medical Journal Publishing Group; 2009;338:b2030. doi: 10.1136/bmj.b2030.

17. Brown J, Wiggins J, Lansdall CJ, Dawson K, Rittman T, Rowe JB. Test Your Memory (TYM test): diagnostic evaluation of patients with non-Alzheimer dementias. J Neurol. 2019;266(10):2546–2553. doi: 10.1007/s00415-019-09447-1.

18. Purvis LAB, Clarke WT, Biasiolli L, Valkovič L, Robson MD, Rodgers CT. OXSA: An open-source magnetic resonance spectroscopy analysis toolbox in MATLAB. PLOS ONE. Public Library of Science; 2017;12(9):e0185356. doi: 10.1371/journal.pone.0185356.

19. Scheltens P, Leys D, Barkhof F, et al. Atrophy of medial temporal lobes on MRI in "probable" Alzheimer's disease and normal ageing: diagnostic value and neuropsychological correlates. J Neurol Neurosurg Psychiatry. 1992;55(10):967–972. doi: 10.1136/jnnp.55.10.967.

20. Fazekas, F. MR signal abnormalities at 1.5 T in Alzheimer's dementia and normal aging. . doi: 10.2214/ajr.149.2.351.

21. An Y, Varma VR, Varma S, et al. Evidence for brain glucose dysregulation in Alzheimer's disease. Alzheimers Dement. 2018;14(3):318–329. doi: 10.1016/j.jalz.2017.09.011.

22. Jeong YJ, Yoon HJ, Kang D-Y. Assessment of change in glucose metabolism in white matter of amyloid-positive patients with Alzheimer disease using F-18 FDG PET. Medicine (Baltimore). 2017;96(48):e9042. doi: 10.1097/MD.0000000000009042.

23. Benzinger TLS, Blazey T, Jack CR, et al. Regional variability of imaging biomarkers in autosomal dominant Alzheimer's disease. Proc Natl Acad Sci. Proceedings of the National Academy of Sciences; 2013;110(47):E4502–E4509. doi: 10.1073/pnas.1317918110.

24. Serés Roig E, De Feyter HM, Nixon TW, et al. Deuterium metabolic imaging of the human brain in vivo at 7 T. Magn Reson Med. 2023;89(1):29–39. doi: 10.1002/mrm.29439.

25. Liu Y, De Feyter HM, Corbin ZA, et al. Parallel detection of multi-contrast MRI and Deuterium Metabolic Imaging (DMI) for time-efficient characterization of neurological diseases. medRxiv. 2023;2023.10.02.23296408. doi: 10.1101/2023.10.02.23296408.

26. Vlassenko AG, Vaishnavi SN, Couture L, et al. Spatial correlation between brain aerobic glycolysis and amyloid-β (Aβ) deposition. Proc Natl Acad Sci U S A. 2010;107(41):17763–17767. doi: 10.1073/pnas.1010461107.

27. Goyal MS, Blazey T, Metcalf NV, et al. Brain aerobic glycolysis and resilience in Alzheimer disease. Proc Natl Acad Sci. Proceedings of the National Academy of Sciences; 2023;120(7):e2212256120. doi: 10.1073/pnas.2212256120.

28. Demetrius LA, Magistretti PJ, Pellerin L. Alzheimer's disease: the amyloid hypothesis and the Inverse Warburg effect. Front Physiol. 2014;5:522. doi: 10.3389/fphys.2014.00522.

29. Newington JT, Harris RA, Cumming RC. Reevaluating metabolism in Alzheimer's disease from the perspective of the astrocyte-neuron lactate shuttle model. J Neurodegener Dis. 2013;2013.

30. Haller S, Zaharchuk G, Thomas DL, Lovblad K-O, Barkhof F, Golay X. Arterial Spin Labeling Perfusion of the Brain: Emerging Clinical Applications. Radiology. 2016;281(2):337–356. doi: 10.1148/radiol.2016150789.

31. Haidar H, Majzoub RE, Hajeer S, Abbas LA. Arterial spin labeling (ASL-MRI) versus fluorodeoxyglucose-PET (FDG-PET) in diagnosing dementia: a systematic review and meta-analysis. BMC Neurol. 2023;23:385. doi: 10.1186/s12883-023-03432-y.

32. Zou C, Ruan Y, Li H, et al. A new deuterium-labeled compound [2,3,4,6,6'-$^{2}H_{5}$]-D-glucose for deuterium magnetic resonance metabolic imaging. NMR Biomed. 2023;36(7):e4890. doi: 10.1002/nbm.4890.

Tables

Table 1: Demographic and clinical characteristics of participants

Characteristic	Participants with AD (n=10)	Control participants (n=9)
Age (y) †	68±5	70±6
Age range (y)	61-77	60-77
Sex		
Males	8 (80.0)	6 (66.7)
Females)	2 (20.0)	3 (33.3)
Cognition score†	ACE-R 66±15	TYM 48±2
Cognition score range	ACE-R 40-86	TYM 46-50
Abnormal cognition	10 (100.0) ‡	0 (0.0) §
MTA (Scheltens' scale)		
Abnormal	8 (80.0)	0 (0.0)
MTA 2	4 (40.0)	
MTA 3	2 (20.0)	
MTA 4	2 (20.0)	
Normal	2 (20.0)	9 (100.0)
MTA 0	1 (10.0)*	3 (33.3)
MTA 1	1 (10.0)**	6 (66.7)
SVD (Fazekas scale)		
Grade 1	7 (70.0)	5 (55.6)
Grade 2	3 (30.0)	4 (44.4)

Note – Unless otherwise specified data are numbers of patients, with percentages in parentheses. AD = Alzheimer's disease, MTA = medial temporal atrophy, ACE-R = Addenbrooke Cognitive Examination Revised (ACE-R), TYM = Test Your Memory cognitive screening test, SVD = small vessel disease.
† Data are means ±standard deviation
‡ 9 participants with AD had ACE-R score of ≤82 (84% sensitivity and 100% specificity for dementia) and one had ACE-R score in 83-88 range (94% sensitivity and 89% specificity for dementia)
§ TYM test was considered normal at scores ≥47 at an age of 60-70 and ≥46 at an age of 70-80

* positive cerebrospinal fluid markers, ** positive ^{18}F-FGD-PET

Figure legends

Fig. 1. Flow diagram showing study participant inclusion. AD = Alzheimer's disease, NIA = National Institute on Aging, TYM = Test Your Memory cognitive screening test.

Fig. 2. Diagram of study timeline. FLAIR = fluid attenuated inversion recovery, p.o. = per os (orally), DMI = deuterium metabolic imaging, MRS = magnetic resonance spectroscopy, MRSI = magnetic resonance spectroscopic imaging.

Fig. 3. Unlocalized (whole-brain) MRS spectra of a control participant and a participant with AD on a clinical 3 T MRI system with peak amplitudes referenced to ^{2}H-water. AD = Alzheimer's disease, MRS = magnetic resonance spectroscopy, ^{2}H-Glx = ^{2}H-glutamate/glutamine.

Fig. 4. Differences in whole-brain MRS metabolite-to-water ratios between participants with AD and control participants. Participants with AD demonstrate a significantly lower ^{2}H-Glx/^{2}H-glucose ratio. AD = Alzheimer's disease, MRS = magnetic resonance spectroscopy, ^{2}H-Glx = ^{2}H-glutamate/glutamine.

Fig. 5. Glucose and metabolite MRSI maps obtained in a participant with AD (67 years old male). Sagittal unenhanced T1-weighted spoiled gradient echo images at the level above corpus callosum (A) and at the level of Sylvian fissures (E), and corresponding MRSI maps of ^{2}H-glucose/^{2}H-water (B and F), ^{2}H-Glx/^{2}H-water (C and G), and ^{2}H-lactate/^{2}H-water (D and H) ratios are shown using a color scale as indicated by the color bars. MRSI images were upscaled by zero filling to generate 2.0 × 2.0 × 3.2 cm voxels and smoothed with a median filter. MRSI = magnetic resonance spectroscopic imaging, ^{2}H-Glx = ^{2}H-glutamate/glutamine.

Figures

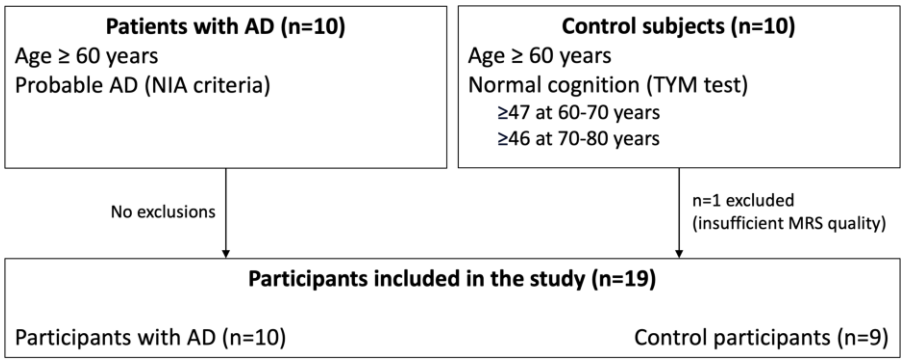

Figure 1

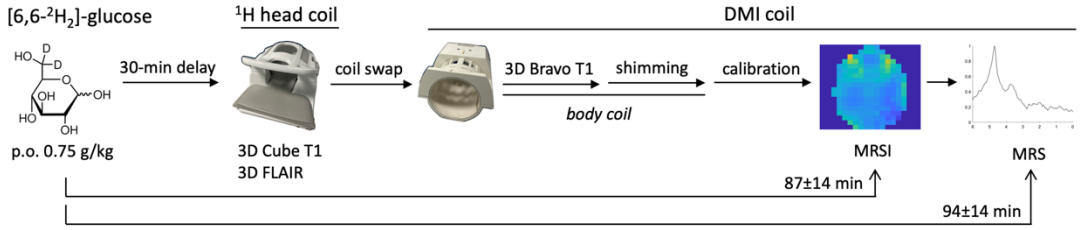

Figure 2

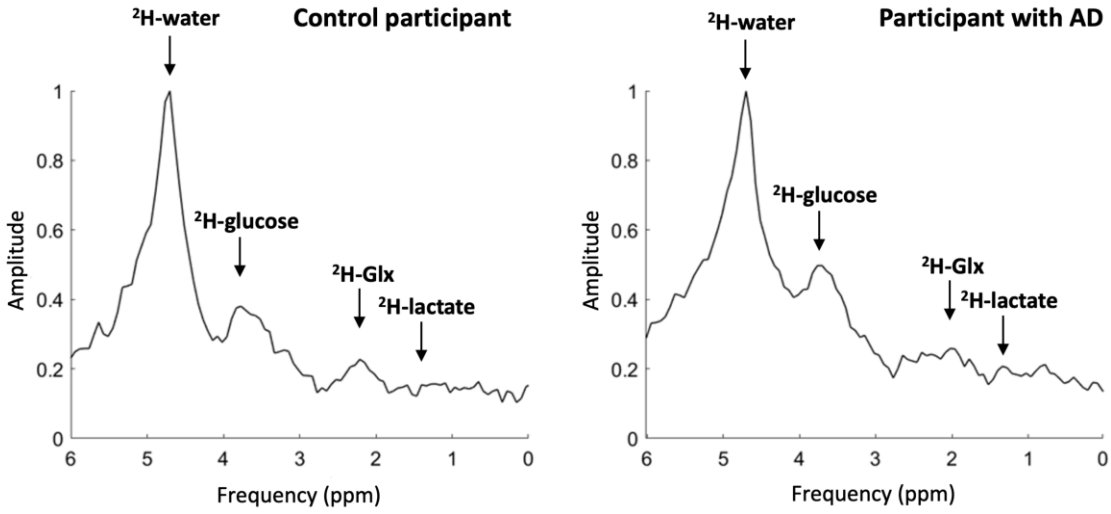

Figure 3

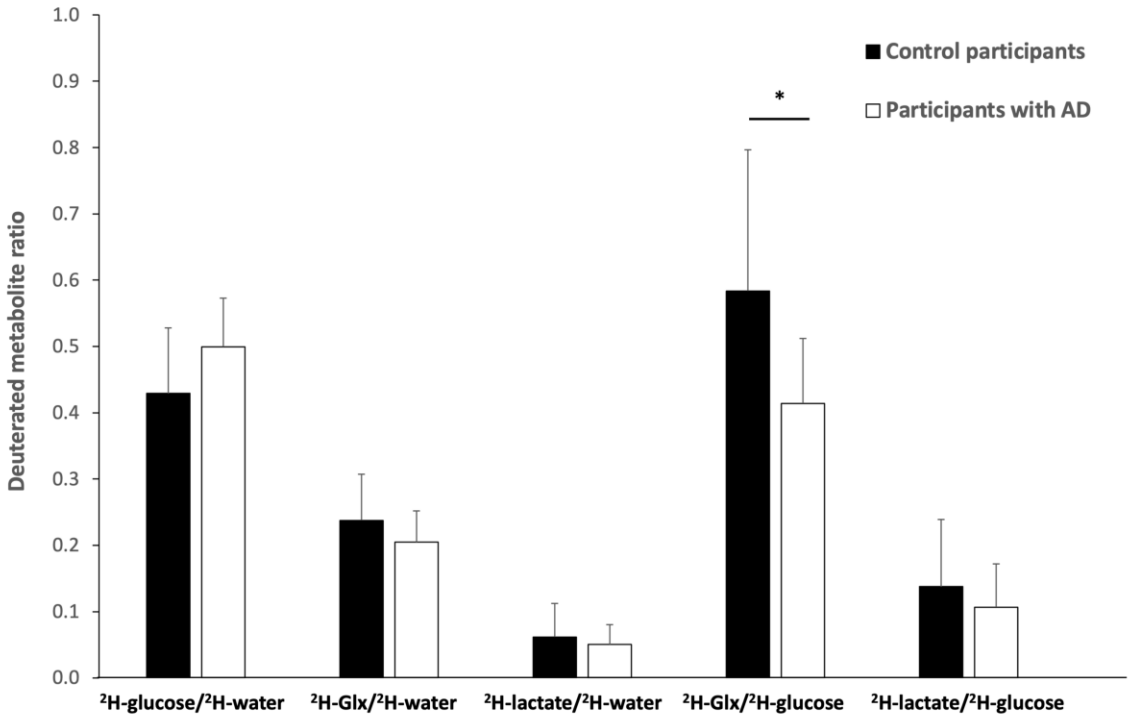

Figure 4

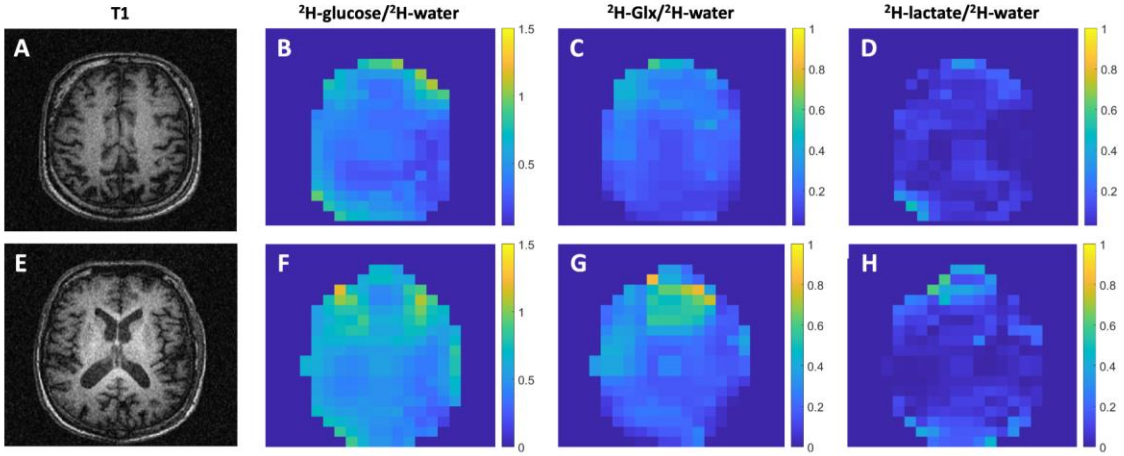

Figure 5

Supplemental Material

Appendix 1

For the analysis of MRSI data, ^{2}H-glucose/^{2}H-water, ^{2}H-Glx/^{2}H-water, ^{2}H-lactate/^{2}H-water, ^{2}H-Glx/^{2}H-glucose, and ^{2}H-lactate/^{2}H-glucose ratios were compared between three MRSI voxels (3.2 x 3.2 x 3.2 cm) overlying the expected areas of glucose metabolism disturbance (bilateral parietal lobes and precuneus) and three voxels overlying the frontal lobes (in which metabolic changes do not usually occur in AD) as a control region in the same MRSI imaging plane superior to the corpus callosum. The voxels overlying the regions of interest were identified by a neuroradiologist (TM, 9 years experience) on T1-weighted spoiled gradient echo images acquired prior to DMI acquisition using the body coil, to which the MRSI maps were referenced. The mean glucose and metabolite-to-water ratios in the selected MRSI voxels were calculated and compared both within (parieto-temporal vs. frontal) and between experimental groups (each region in participants with AD vs. healthy participants).

For atlas-based segmentation, the sagittal 3D Cube T1-weighted images acquired with the proton head coil were co-registered to the T1-weighted spoiled gradient echo images obtained with the body coil (and therefore to the aligned MRSI maps) using FSL routines (Woolrich MW et al, Neuroimage, 2009; 45:S173-86). Registered sagittal 3D Cube T1-weighted images were subsequently segmented using a modified Hammers brain atlas (Hammers A et al, Human Brain Mapp 2003, 19: 224-247). Due to the limitations associated with the large size of the source MRSI data voxels, the Hammers atlas fields were merged to to obtain larger areas of interest in which glucose hypometabolism would be expected - parietal lobe (merger of the superior parietal gyrus, supramarginal gyrus, and angular gyrus fields) and the lateral aspect of the temporal lobe (merger of the superior, middle and inferior temporal gyri and posterior temporal lobe), and areas of presumed normal metabolism - frontal lobe (merger of the superior and middle frontal gyri) and occipital lobe (merger of the angular gyrus and lateral remainder occipital lobe). DMI values were extracted from bilateral regions of interest and the mean ^{2}H-glucose/^{2}H-water, ^{2}H-Glx/^{2}H-water, ^{2}H-lactate/^{2}H-water, ^{2}H-Glx/^{2}H-glucose, and ^{2}H-lactate/^{2}H-glucose ratios were calculated. The values were compared both within (all regions of interest individually, as well as combined parietal plus temporal vs. combined frontal plus occipital lobe) and each region across experimental groups (participants with AD vs. healthy participants).

There was no evidence of a difference in metabolite levels between selected brain regions using either way of analysis. The table below demonstrates values of metabolic ratios (mean±SD) obtained from the parietal and frontal voxels with corresponding *P* values for comparisons within (parietal vs. frontal) or across (participant with AD vs control participants) groups.

Metabolite / region	**Control participants**	**Participants with AD**	***P* (AD vs control)**
^{2}H-glucose/^{2}H-water			
parietal	0.33 ± 0.12	0.33 ± 0.16	
frontal	0.33 ± 0.09	0.31 ± 0.15	.98
P (parietal vs frontal)	.97	.87	.92
^{2}H-Glx/^{2}H-water			.50
parietal	0.16 ± 0.06	0.14 ± 0.04	.48
frontal	0.18 ± 0.07	0.15 ± 0.05	
P (parietal vs frontal)	.14	.32	
^{2}H-lactate/^{2}H-water			.66
parietal	0.05 ± 0.03	0.05 ± 0.04	.90
frontal	0.04 ± 0.03	0.04 ± 0.03	
P (parietal vs frontal)	.81	.84	
^{2}H-Glx/^{2}H-glucose			.93
parietal	0.53 ± 0.22	0.55 ± 0.30	.84
frontal	0.54 ± 0.15	0.52 ± 0.31	
P (parietal vs frontal)	.87	.58	
^{2}H-lactate/^{2}H-glucose			.72
parietal	0.14 ± 0.05	0.16 ± 0.13	.37
frontal	0.13 ± 0.12	0.13 ± 0.07	
P (parietal vs frontal)	.84	.40	

Similarly, there was no evidence of a difference in metabolite levels in regions identified using the modified brain atlas, either between different brain regions (*P*=.09 to .89) or between participants with AD vs control participants (*P*=.07 to .97).

Supplemental Table 1:

Individual demographic data, cognition scores (ACE-R score and sub-scores for patients and TYM score for control subjects), medial temporal atrophy score (MTA) and small vessel disease (SVD, Fazekas scale) in the study participants.

AD patients

ID	Age	Sex	ACE-R [sub-scores]	MTA	SVD	Comments
1	68	M	79 [18-14-8-25-14]	4	1	Positive cerebrospinal fluid markers†
2	61	F	56 [9-7-6-23-11]	2	1	-
3	62	M	37 [8-5-4-18-2]	2	1	Presenilin-1 mutation
4	77	M	70 [18-11-6-20-15]	3	2	-
5	66	M	69 [14-14-10-22-9]	2	2	-
6	67	M	78 [18-12-10-25-13]	3	1	-
7	70	M	49 [8-6-4-23-8]	2	1	-
8	56	M	71 [17-13-7-23-11]	1	2	Positive 18F-FDG PET‡
9	73	M	59 [13-11-4-15-16]	4	1	-
10	68	F	86 [18-16-12-25-15]	0	1	Positive cerebrospinal fluid markers†

Control subjects

ID	Age	Sex	TYM	MTA	SVD
1	69	M	50	1	1
2	72	M	46	0	2
3	60	M	48	0	1
4	66	F	50	1	1
5	63	M	49	1	1
6	75	F	48	1	2
7	73	M	50	0	1
8	77	M	47	1	2
9	76	F	47	1	2

† Aβ1-42 < 627 pg/ml, total Tau > 595 pg/ml, total Tau/Aβ ratio > 1 (local clinical reference values)
‡ clinical report of reduction of 18F-FDG uptake in temporo-parietal regions and the precuneus typical for AD

ACE-R sub-scores are given for [attention and orientation-memory-fluency-language-visuospatial] domains (maximum achievable scores of 18-26-14-26-16 respectively). The ACE-R test was not repeated on the day of the scan, but scores obtained at the most recent memory clinic were provided (on average two months before the scan).

ACE-R score of ≤88 has 94% sensitivity and 89% specificity for dementia

ACE-R score of ≤82 has 84% sensitivity and 100% specificity for dementia (15)

MTA scores ≥2 in patients <75 years of age, or scores of 3 and 4 at any age were considered abnormal

(Barkhof F 2011. Neuroimaging in dementia. Springer Verlag)

TYM test was performed in control participants on the day of the scan and was considered normal at scores ≥47 at an age of 60-70 and ≥46 at an age of 70-80

Negative predictive value of TYM test is 99% for AD (16) and 84% for non-AD dementia at a threshold of 42 (17)

Supplemental Table 2:

Correlation coefficients and two-tailed p values for correlations between ACE-R or MTA scores and metabolite ratios in patients with AD.

	^{2}H-glucose / ^{2}H-water	^{2}H-Glx / ^{2}H-water	^{2}H-lactate / ^{2}H-water	^{2}H-Glx / ^{2}H-glucose	^{2}H-lactate / ^{2}H-glucose
ACE-R					
r	-0.49	-0.09	0.59	0.18	0.58
P	0.15	0.80	0.09	0.61	0.08
MTA					
rs	-0.24	0.18	0.41	0.14	0.39
P	0.50	0.61	0.14	0.70	0.16

Dependence between continuous variables (ACE-R and metabolite ratios) was tested using Pearson's correlation.

Pearson's correlation coefficient (r) and significance (*P)* values are listed

Dependence between discrete (MTA) and continuous variables (metabolite ratios) was tested using Spearman's correlation.

Spearman's correlation coefficient (rs) and significance (*P*) values are listed